Solar Energy Materials & Solar Cells 295 (2026) 113978

Contents lists available at ScienceDirect

Solar Energy Materials and Solar Cells

journal homepage: www.elsevier.com/locate/solmat

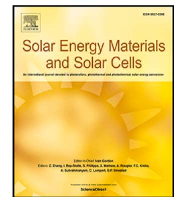

On the impact of lateral inhomogeneity on photoconductance decay lifetime measurements ☆

Axel Herguth *, Alexander Graf

University of Konstanz, Department of Physics, Universitätstrasse 10, Konstanz, 78464, Germany

ARTICLE INFO

Keywords:
Photoconductance decay (PCD)
Silicon
Excess carrier lifetime
Characterization technique

ABSTRACT

The photoconductance decay technique is commonly used to measure the injection-dependent effective lifetime of excess charge carriers in crystalline silicon allowing for an in-depth analysis of excess charge carrier recombination. Its working principle relies on eddy currents induced by a coil within a certain sensitivity region in which the sample properties, in particular the excess charge carrier lifetime, should be homogeneous as the technique only yields a laterally integrated result. Within this paper it is discussed in theory, simulation and experiment how lateral inhomogeneity of excess charge carrier lifetime impacts the result of the lifetime measurement. It is shown that extended regions of strongly different bulk lifetime result in abnormal injection-dependent lifetime curves whose shape depends on the applied measurement and analysis conditions. Experimental results hereby validate the presented theoretical approach. It is furthermore discussed, how continuous distributions of lifetime, like a lateral gradient in lifetime, may conceal to some degree the abnormal shape and may lead to erroneous analysis results. Finally it is demonstrated that lateral inhomogeneous surface passivation results in distorted lifetime curves as well.

1. Introduction

The (effective) excess charge carrier lifetime is a key factor in silicon wafer-based solar cells. It is impacted by various aspects, in particular defects in the bulk and passivation of the surfaces. Unfortunately, the complex nature of solar cells architecture, being at least two- if not three-dimensional due to the metallization pattern, complicates the analysis of specific aspects regarding excess charge carrier lifetime. It is therefore common practice, to investigate simpler 'lifetime structures' instead consisting only of the substrate and passivation layers. These lifetime structure are mostly treated as zero-dimensional structures as (i) photoconductance decay (PCD) measurements [1–3] commonly used for the quantification of excess carrier lifetime yield only thickness-averaged values anyway, and (ii) structures are made and assumed to be laterally homogeneous at least within the sensitivity region of the PCD tool. For reference, for the widely used eddy-current-based lifetime tester from Sinton Instruments this is a ring-like region roughly 30 mm in diameter [4–6].

Simply due to the lack of spatially resolved information and analysis techniques to deal with such information, and sometimes also due to a lack of awareness of potential inhomogeneity, effective excess charge carrier lifetime is often regarded as an easy-to-interpret global property. Reality, however, looks often different. Multicrystalline material is of course by definition inhomogeneous but even monocrystalline samples suffer from lateral inhomogeneity due to practically unavoidable growth-related ring-like structures (see Fig. 1) and imperfect processing (diffusions, layer depositions, heat treatments etc.). Sometimes these effects only become visible after degradation (again see Fig. 1) revealing lateral differences in hydrogenation among other things. To make it worse, scratches and insufficiently passivated edges impact samples as well.

Within this contribution, it is explained in theory, simulation and experiment how this affects laterally averaged photoconductance decay (PCD) measurements and how it affects the analysis of injection dependence.

2. Theoretical background

During a PCD measurement, the conductance of a sample is measured by eddy-currents induced by a short coil underneath the sample which is part of a high frequency oscillating circuit operated at some MHz. From laterally integrated conductivity σ the optically-excited excess charge carrier concentration or injection Δn (assuming neutrality, i.e. the excess of electrons equals that of holes $\Delta n = \Delta p$) compared to equilibrium electron and hole concentrations n_0 and p_0 (without optical

☆ This article is part of a Special issue entitled: 'SiliconPV 2025' published in Solar Energy Materials and Solar Cells.

* Corresponding author.
E-mail address: axel.herguth@uni-konstanz.de (A. Herguth).

https://doi.org/10.1016/j.solmat.2025.113978
Received 27 June 2025; Accepted 20 September 2025
Available online 14 October 2025
0927-0248/© 2025 The Authors. Published by Elsevier B.V. This is an open access article under the CC BY license (http://creativecommons.org/licenses/by/4.0/).

Konstanzer Online-Publikations-System (KOPS)
URL: http://nbn-resolving.de/urn:nbn:de:bsz:352-2-1fvxgufbwl6v60

excitation) can be calculated with known mobilities of electrons and holes μ_n and μ_p, and elementary charge q according to

$$\sigma = q \cdot \left[\mu_n \cdot (n_0 + \Delta n) + \mu_p \cdot (p_0 + \Delta n)\right] \quad (1)$$

$$\approx q \cdot \mu_p \cdot p_0 + q \cdot (\mu_n + \mu_p) \cdot \Delta n \quad (2)$$

where the second line of the above equation is simplified here for the case of p-type material with $p_0 \gg n_0$. Actually, only the excess conductivity implied by the Δn term is used, but note that mobilities have to be evaluated at the overall charge carrier concentrations. Hence, excess conductivity is neither independent of p_0 nor Δn, however, for the sake of simplicity this is neglected in the following. Effective lifetime τ_{eff} is derived from the well-known equation [3]

$$\tau_{\text{eff}} = \frac{\Delta n}{G - \frac{d\Delta n}{dt}} \quad (3)$$

which can be used to extract τ_{eff} either (i) in the case of generation $G(t)$ slowly decaying in time commonly referred to as quasi steady state (QSS) mode ($d\Delta n/dt \ll G$), or (ii) in the case of a transient decay of Δn without further generation after initial excitation ($G \ll d\Delta n/dt$) commonly referred to as transient (TRA) mode. A generalized (GEN) mode exploiting Eq. (3) is also possible and advisable [3] but this paper shall focus on the extreme QSS and TRA cases first and discuss the GEN case afterwards.

In order to understand how lateral inhomogeneity impacts a PCD lifetime measurement in the different modes, consider for simplicity that a sample has two extended regions H (high lifetime) and L (low lifetime) with specific injection-dependent effective lifetimes $\tau_H(\Delta n_H)$ and $\tau_L(\Delta n_L)$, and that lateral transport is negligible. Such a sample was prepared experimentally (discussed later on) and a photoluminescence image is shown in Fig. 1. Integral conductivity of a mixed (M) region σ_M of such a sample can be written as the sum of conductivities σ_H and σ_L in the individual regions weighted by their respective areal fraction f_H and f_L inside the sensitivity region.

$$\sigma_M = f_H \cdot \sigma_H + f_L \cdot \sigma_L \quad (4)$$

where $f_H + f_L = 1$. Ignoring the issue that mobilities will slightly differ in the respective regions when the overall carrier concentrations differ, this can be simplified to an overall injection Δn_M given by

$$\Delta n_M = f_H \cdot \Delta n_H + f_L \cdot \Delta n_L \quad (5)$$

$$= \tfrac{1}{2} \cdot \left(\Delta n_H + \Delta n_L\right) \quad \text{for} \quad f_H = f_L = \tfrac{1}{2} \quad (6)$$

For the sake of simplicity, equal areal fractions for the mixed region are assumed in the following. Note that the above equation represents the situation at every time or, in other words, mixing occurs in the time domain (not in the injection domain!). What happens during the PCD measurement now depends on the mode of operation.

2.1. Quasi steady state mode (QSS)

In QSS mode, apparent effective lifetime follows from $\tau_M = \Delta n_M/G$ (Eq. (3) for $d\Delta n/dt \ll G$). This implies that at an integral injection of

$$\Delta n_M(t) = \tfrac{1}{2} \cdot \left[\Delta n_H(t) + \Delta n_L(t)\right] \quad (7)$$

a lifetime

$$\tau_M(t) = \tfrac{1}{2} \cdot \left[\tau_H(t) + \tau_L(t)\right] \quad (8)$$

will be measured. How this might look like for the situation in Fig. 1 is demonstrated in Fig. 2 by means of a simulation. In a first step, injection-dependent lifetime curves $\tau_H(\Delta n_H)$ and $\tau_L(\Delta n_L)$ were calculated assuming a p-type material doped with $1 \cdot 10^{16}\,\text{cm}^{-3}$ with similar surface limitation ($J_{0,\text{srf}} = 10\,\text{fA}\,\text{cm}^{-2}$), and in both cases a SRH defect with a τ_p/τ_n ratio of 30 (typical for LeTID ranging from 20 to 36 [7–13]), however, with a different τ_n value of either 70 µs or 10 µs. This roughly reproduces the situation in Fig. 1 as discussed later on in

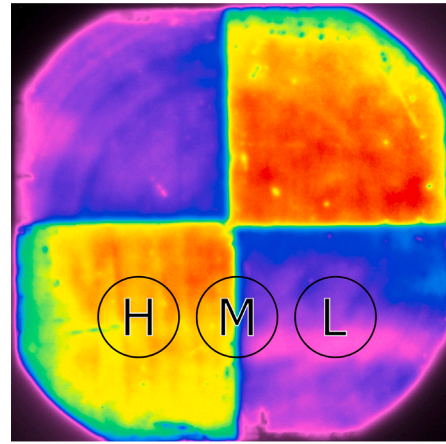

Fig. 1. Photoluminescence image of a Cz–Si sample (size 156 mm) prepared to exhibit regions of distinctively different excess charge carrier lifetimes by means of masking during a regeneration treatment. Redish regions feature a rather high effective lifetime while bluish regions are of low lifetime. The positions/sensitivity regions of measurements are highlighted.

more detail. Intrinsic recombination was taken into account with state-of-the-art models [14], however, lifetime is limited by surface and SRH recombination anyway. The resulting $\tau_H(\Delta n_H)$ and $\tau_L(\Delta n_L)$ are shown in the bottom part of Fig. 2 as thick gray lines. In a second step the PCD measurement was simulated in a time-resolved manner assuming a rather slow decaying generation G. This was done for the individual regions ($f_H = 1$ or $f_L = 1$). The resulting 'measured' lifetime curves τ_H and τ_L are shown as colored lines and the perfect agreement with the assumed lifetime curves in the different regions proves the validity of the analysis done in QSS mode. The upper part of Fig. 2 shows what happens in the time domain in the individual regions and in the mixed region. The coloring of data is chosen to reflect time allowing to visualize timing also in the injection domain. Decay of injection in the mixed region does not look noticeably different from the individual regions. However, lifetime in the mixed region $\tau_M(t)$ looks somewhat strange with its two maxima during the orange and green phase of the PCD measurement being a result of differently timed maxima in $\tau_H(t)$ and $\tau_L(t)$. Those maxima reflect the fact that the PCD measurement (running from high to low injection as time progresses) starts at such a high injection in the individual regions that effective lifetime first increases with dropping injection (generation) due to surface limitation before it drops due to SRH limitation. Both, τ_H and τ_L run through this maximum but at different points in time; $\tau_H(t)$ does it significantly later (green phase) than $\tau_L(t)$ does (red phase). This double maximum in $\tau_M(t)$ can then also be found in the resulting $\tau_M(\Delta n_M)$ curve. A look on the color coding in the bottom part of Fig. 2 nicely demonstrates that averaging does not occur in the injection domain even though τ_M approaches the average value $\tfrac{1}{2} \cdot (\tau_H + \tau_L)$ for low injection where the individual lifetime curves flatten out. That both maxima are on the same level, producing a virtual plateau, is rather coincidental and related to the specific choice of τ_n and area fraction $f_L = \tfrac{1}{2}$. A look to Fig. 12 in the appendix shows that this is not necessarily the case if the area fractions of the high and low lifetime region are changed. Depending on the choice of f_L one of the maxima may also appear rather as a shoulder than as a clear maximum.

2.2. Transient mode (TRA)

The situation is somewhat different in TRA mode. Effective lifetime follows from $\tau_{\text{eff}} = -\Delta n/(d\Delta n/dt)$ (Eq. (3) for $d\Delta n/dt \gg G$) with the derivative being negative as Δn decays. At an integral injection of

$$\Delta n_M(t) = \tfrac{1}{2} \cdot \left[\Delta n_H(t) + \Delta n_L(t)\right] \quad (9)$$

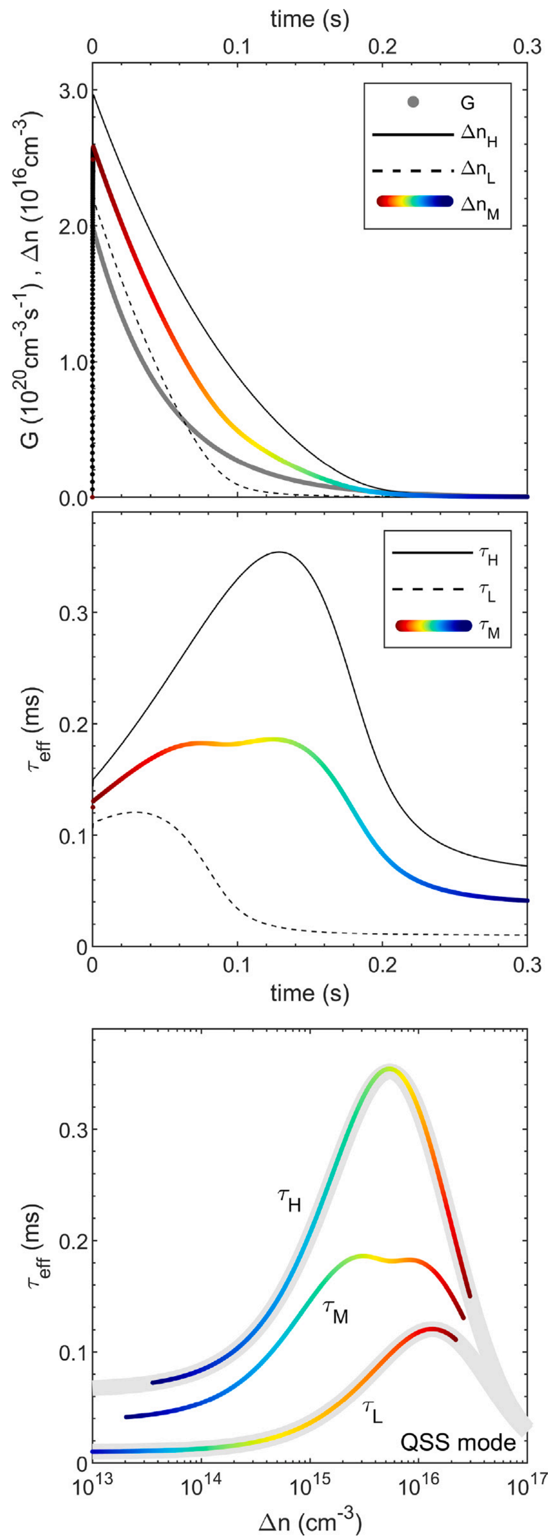

Fig. 2. Results from a simulation of a PCD measurement and its analysis in QSS mode. Coloring reflects the progress in time. (top) Time-resolved generation G, injection Δn and effective lifetime τ_{eff} in the regions of high and low lifetime H and L and in the mixed region M. (bottom) Resulting injection-dependent effective lifetime curve $\tau_{\mathrm{eff}}(\Delta n)$. The thick gray curves show the assumed lifetime curves in the regions of low ($\tau_{\mathrm{n}} = 10\,\mu\mathrm{s}$) and high lifetime ($\tau_{\mathrm{n}} = 70\,\mu\mathrm{s}$).

a lifetime

$$\tau_{\mathrm{M}}(t) = -\frac{\frac{1}{2} \cdot \left(\Delta n_{\mathrm{H}} + \Delta n_{\mathrm{L}}\right)}{\frac{1}{2} \cdot \left(\frac{d\,\Delta n_{\mathrm{H}}}{dt} + \frac{d\,\Delta n_{\mathrm{L}}}{dt}\right)} \tag{10}$$

is measured. The factor $\frac{1}{2}$ of course cancels out, however, it is worth noting that it is present in both, Δn_{M} and its derivative, and that its occurrence in the latter results in the step-like behavior discussed later. In order to study the effect of lifetime mixing, a PCD measurement in TRA mode was simulated using the same sample parameters as before, however, a much shorter generation was chosen to ensure a transient decay of injection suited for TRA analysis undisturbed by residual generation. The perfect match of "measured" (colored lines) and assumed lifetime (thick gray lines) in the individual regions in Fig. 3 proves that the TRA analysis works as expected. Again the coloring reflects the progress in time. A look on the decay of injection in the upper part of Fig. 3 shows a peculiarity. In the blue phase, there is a rather abrupt change in slope in Δn_{M} visible as a step in its derivative that occurs once Δn_{L} vanishes. This step in the blue phase transfers to the injection-dependent lifetime curve $\tau_{\mathrm{M}}(\Delta n_{\mathrm{M}})$ which also demonstrates that the individual regions progress differently in time through injection. It is interesting to see that τ_{M} even exceeds τ_{H} towards low injection after this step. This can be understood with view to Eq. (10) which simplifies in the blue phase to

$$\tau_{\mathrm{M}} \approx -\frac{\Delta n_{\mathrm{H}}}{\frac{d\,\Delta n_{\mathrm{H}}}{dt}} \mathrel{\widehat{=}} \tau_{\mathrm{H}} \tag{11}$$

after Δn_{L} has vanished. So, in principle $\tau_{\mathrm{M}}(t)$ converges to $\tau_{\mathrm{H}}(t)$. However, Δn_{M} does not equal Δn_{H} but $\frac{1}{2} \cdot \Delta n_{\mathrm{H}}$ instead. Hence, τ_{M} mimics τ_{H} but with a shifted injection, and as τ_{H} drops in this injection range, $\tau_{\mathrm{M}}(\Delta n_{\mathrm{M}})$ is pushed above $\tau_{\mathrm{H}}(\Delta n_{\mathrm{H}})$. Once τ_{H} flattens out towards low injection, this difference in injection becomes insignificant and it looks as if τ_{M} converges to τ_{H}. In this context it is also worth to note how the area fraction f_{L} of the low lifetime region impacts the PCD measurement in TRA mode as it is depicted in Fig. 13 in the appendix. Regardless of the choice of f_{L}, τ_{M} does never exceed the maximum value of $\tau_{\mathrm{H}}(\Delta n_{\mathrm{H}})$. It is rather the position of the step that shifts in injection. If the high lifetime region only makes up a tiny area fraction, like 1 % (black line in Fig. 13), one might be tempted to dismiss the increase towards low injection as the result of minority carrier trapping [15] also causing a delayed decay of excess conductivity. At first glance, there are some similarities as the lifetime region locally retains excess conductivity, but in contrast to trapping where only excess majority carriers contribute to excess conductivity, both excess minority and majority carriers contribute to excess conductivity in the high lifetime region. However, it should be noted that the impact of such small area fractions might not be well described with the above theory since charge carrier diffusion between regions with different lifetimes/injection likely becomes more important as the regions become smaller.

2.3. Generalized mode (GEN)

How close the measured lifetime in QSS and TRA mode comes to the 'true' τ_{eff} depends on the ratio of τ_{eff} and flash duration t_{f} (with the flash modeled as single-exponential decay). Nagel et al. [3] conclude that the evaluation in the intermediate range, where t_{f} is between $10 \cdot \tau_{\mathrm{eff}}$ (a suggested upper τ_{eff} limit for the QSS mode) and $0.4 \cdot \tau_{\mathrm{eff}}$ (a suggested lower τ_{eff} limit for the TRA mode), is especially prone to error. In the simulations described above, this was guaranteed with t_{f} being either 50 ms (QSS, Fig. 2) or 1 µs (TRA, Fig. 3). In reality, however, using the aforementioned commonly used tool from Sinton Instruments, the flash duration cannot be adjusted at will. Either a long flash with $t_{\mathrm{f}} \approx 2$ ms or a short flash with $t_{\mathrm{f}} \approx 25\,\mu$s can be selected. Following the suggestions above, neither lifetimes above ~200 µs should be measured in QSS mode nor lifetimes below ~60 µs should be measured in TRA

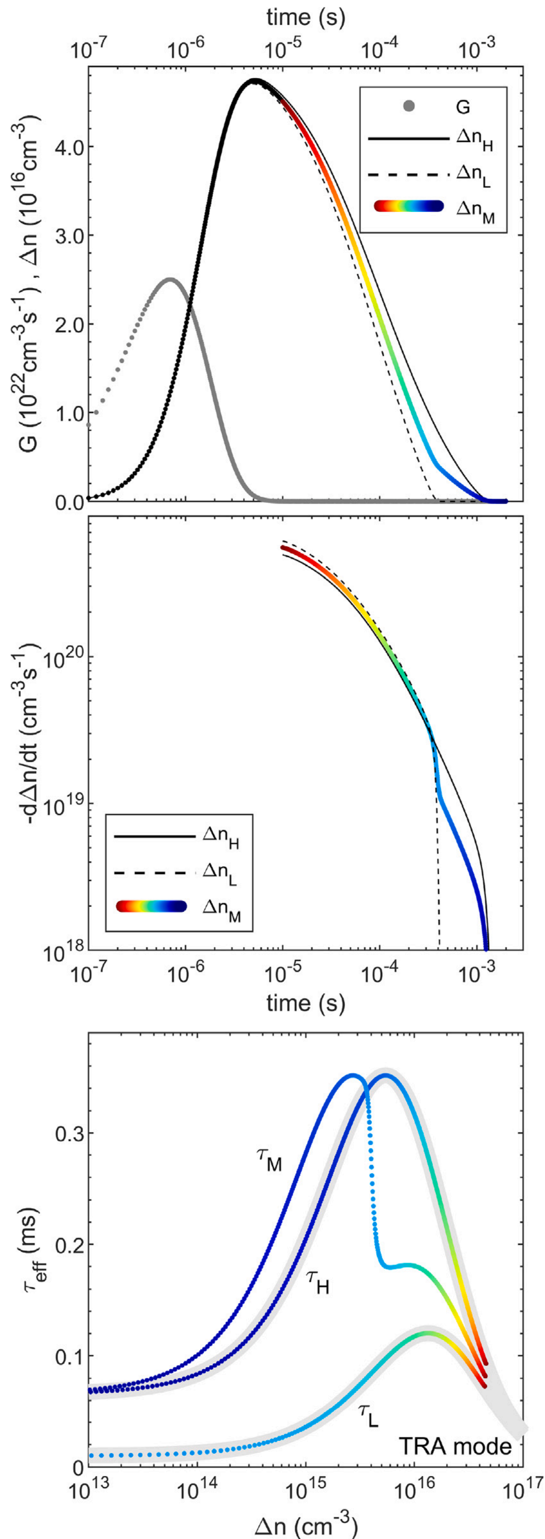

Fig. 3. Results from a simulation of a PCD measurement and its analysis in TRA mode. Coloring reflects the progress in time. (top) Time-resolved generation G, injection Δn and its (absolute) change with time $d\Delta n/dt$ in the regions of high and low lifetime H and L and in the mixed region M. (bottom) Resulting injection-dependent effective lifetime curve $\tau_{\mathrm{eff}}(\Delta n)$. The thick gray curves show the assumed lifetime curves in the regions of low ($\tau_{\mathrm{n}} = 10\,\mu\mathrm{s}$) and high lifetime ($\tau_{\mathrm{n}} = 70\,\mu\mathrm{s}$).

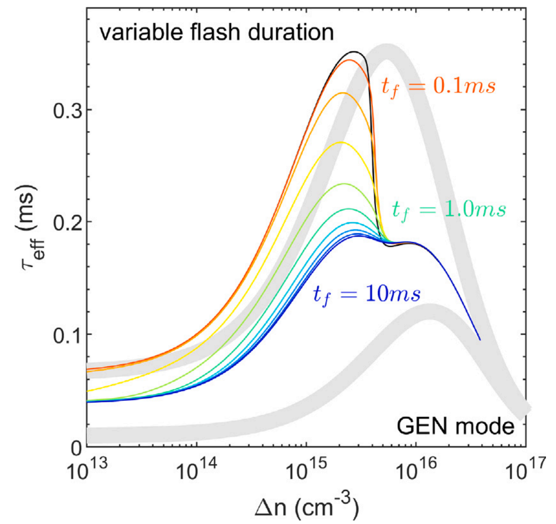

Fig. 4. Results of the simulated lifetime measurements in GEN mode in the mixed case ($f_{\mathrm{L}} = f_{\mathrm{H}} = \frac{1}{2}$) with variable flash duration t_{f}. The black curve represents the result with the $1\,\mu\mathrm{s}$ flash used for the TRA analysis in Fig. 3. Flash durations are chosen equidistant on logarithmic scale with four lines per decade. For comparison, the gray curves show the assumed lifetime curves in the regions of low ($\tau_{\mathrm{n}} = 10\,\mu\mathrm{s}$) and high lifetime ($\tau_{\mathrm{n}} = 70\,\mu\mathrm{s}$).

mode whereby it should be noted that lifetime may vary with injection, so that parts of the modeled $\tau_{\mathrm{eff}}(\Delta n)$ curves should actually be measured in TRA mode while others should be measured in QSS mode. This is where a generalized (GEN) analysis based on Eq. (3) is advised [3]. Of course, there has to be a transition between the τ_{M} curves shown in Fig. 2 (QSS mode) and Fig. 3 (TRA mode) when flash duration t_{f} falls in the range of τ_{eff}. In order to investigate this in detail, again PCD simulations were done with the same sample properties as before, but with a variable flash duration t_{f} implemented as $G(t) = G_0 \cdot \exp(-t/t_{\mathrm{f}})$. The resulting lifetime curves in the mixed region ($f_{\mathrm{L}} = f_{\mathrm{H}} = \frac{1}{2}$) are shown in Fig. 4 color-coded with flash duration. As can be seen, the GEN analysis begins to deviate from the TRA measurement (black line, identical to Fig. 3) when t_{f} exceeds $0.1\,\mathrm{ms}$ and becomes comparable with lifetime in the high lifetime region. Even though the step around $\Delta n \approx 4 \cdot 10^{15}\,\mathrm{cm}^{-3}$ gets washed out to some degree with increasing flash duration, the step still remains visible. What changes noticeably is the behavior in low injection. While lifetime converges to the high lifetime curve in TRA mode, it converges in GEN mode to the arithmetic mean found in QSS mode even though the step known from TRA mode is still present. Hence, the measurement in GEN mode may show features from both, QSS and TRA mode, making an analysis even more complex.

3. Experimental validation

In order to validate the theory and simulations discussed before, a proof-of-principle experiment was performed. A boron-doped Cz–Si wafer with an edge length of 156 mm was etched and cleaned wet-chemically before an hydrogen-rich amorphous silicon nitride layer (SiN_x:H) was deposited by plasma-enhanced chemical vapor deposition on front and rear as surface passivation and as a source of hydrogen. The sample was fired in a belt furnace in order to drive hydrogen into the silicon bulk. Note that boron-doped, oxygen-rich and hydrogen-enriched Cz–Si is susceptible to boron–oxygen related degradation (BOLID) [16,17] and light- and elevated temperature induced degradation (LeTID) [18] when exposed to illumination and elevated temperatures, but may also regenerate these degradation losses for prolonged exposure. This was exploited to create the sample shown in Fig. 1. Two quarters of the sample were covered with silicon wafer pieces to suppress but eventually not completely block illumination.

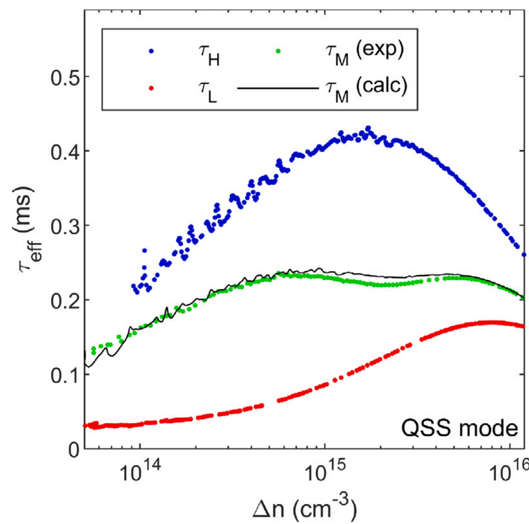

Fig. 5. Results of the lifetime measurements in QSS mode of the sample shown in Fig. 1 in the individual regions H and L and in the mixed region M. Also shown is the calculated curve τ_M(calc) for the mixed region using τ_H and τ_L and equal area fractions $f_H = f_L = \frac{1}{2}$.

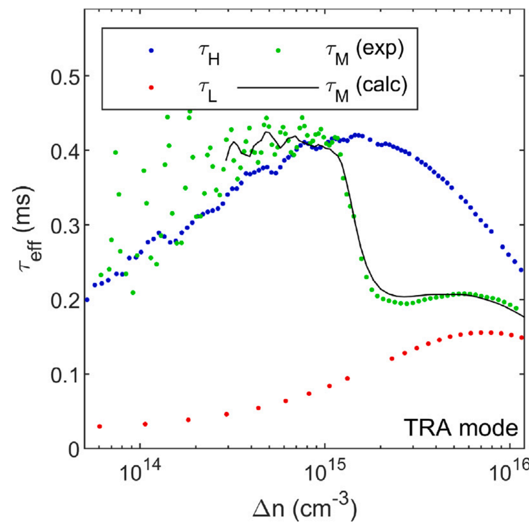

Fig. 6. Results of the lifetime measurements in TRA mode of the sample shown in Fig. 1 in the individual regions H and L and in the mixed region M. Also shown is the calculated curve τ_M(calc) for the mixed region using τ_H and τ_L and equal area fractions $f_H = f_L = \frac{1}{2}$.

The sample was then exposed to illumination equivalent to 1 sun at 110 °C for 24 h. In the un-masked areas, both BOLID and LeTID are expected to occur and at least partially regenerate resulting in a rather high lifetime region. A look on the injection-dependent lifetime curves shown in Figs. 5/6 suggests that lifetime is still limited to some degree towards low injection, but a SRH analysis did not yield a conclusive result whether this is due to BOLID or LeTID or another defect species. Note however, that this is not of importance here anyway. In the masked regions, at least LeTID is expected to occur, but on a longer timescale, hence leaving this area in a degraded state with low lifetime. A SRH analysis points towards LeTID as limiting factor.

The results from lifetime measurements taken in either QSS or TRA mode are shown in Fig. 5 and Fig. 6, respectively. Note that effective lifetime either in the H or L region is not well suited for one of the modes, but that the resulting lifetimes curves in the H and L region are in good agreement nevertheless. The choice of an unsuitable mode

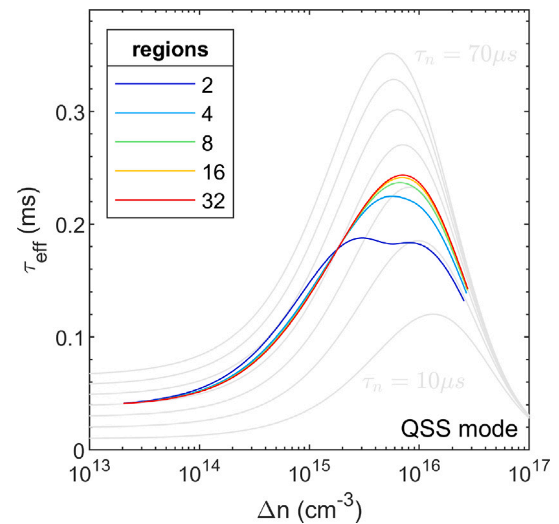

Fig. 7. Results of the simulated lifetime measurements in QSS mode of a sample with a variable number of regions of equal area each exhibiting a lifetime τ_n in between 10 and 70 μs equidistantly spaced. The case of two regions (blue) corresponds to Fig. 2. A selection of individual lifetime curves is shown in gray in steps of 10 μs for comparison.

is therefore not considered to be the cause of the 'abnormal' curves in the mixed region. The 'abnormal' curves rather validate the above discussed theory, with the QSS measurement reproducing the double maximum, and the TRA measurement reproducing the step with τ_M exceeding τ_H even though the data are quite noisy there. In addition, the lifetime curves for the mixed region (solid lines) calculated with the above theory using the $\Delta n(t)$ data in the H and L region are in good agreement with the measured data. With view to Fig. 12, some disagreement in QSS mode might be related to not well-defined area fractions. In addition, the contribution of the area affected by lateral diffusion in between the high and low lifetime region is neglected.

4. Lifetime gradients

The abnormal curve shape of τ_M in Figs. 5/6 is easy to recognize. However, in reality samples will probably not show such a clear pattern like Fig. 1 but likely a more gradual, continuous distribution of lifetimes. In order to investigate how this impacts PCD measurements, a step-wise evolution from just 2 regions to 2^n regions was simulated. In all regions of equal size, τ_n assumes equidistant values in between 10 and 70 μs while all other parameters remain the same. Again, PCD measurements in QSS and TRA mode are simulated and the resulting lifetime curves are shown in Fig. 7 and Fig. 8, respectively. As can be seen, the double maximum observed in QSS mode for just 2 regions vanishes and the lifetime curves do not look suspicious at first glance. However, a comparison with the set of lifetime curves with the same defect parameters but different τ_n (gray lines) shows that the resulting lifetime curves do not behave like the underlying defect suggests. Starting at 40 μs (the arithmetic mean of 10 and 70 μs), the simulated lifetime curve increases stronger than the gray curve suggesting a higher τ_p/τ_n ratio. But this strong initial increase weakens afterwards and the lifetime curves crosses towards the gray 30 μs curve suggesting a lower τ_p/τ_n ratio. Fitting such a lifetime curve with a single SRH defect does not work.

In TRA mode depicted in Fig. 8, the situation is even worse. As the number of regions increases, more and more steps occur, actually $2^n - 1$, but their amplitude decreases. Finally, the lifetime curve smoothes out and apart from a small ripple around $7 \cdot 10^{15}$ cm^{-3} the red curve does not look suspicious. However, a comparison with the gray lines of variable τ_n shows the large deviation. Starting at 70 μs, the simulated curve lies

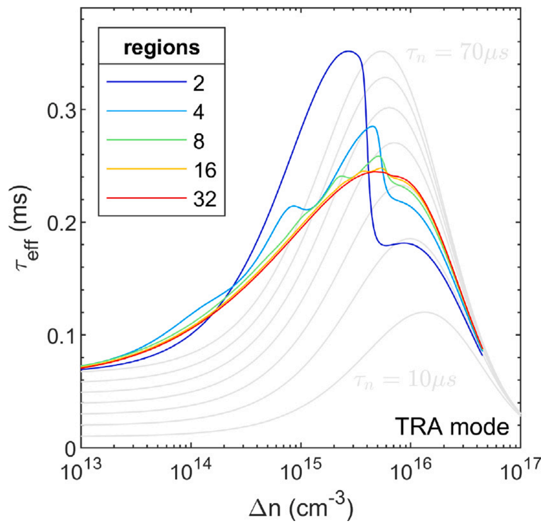

Fig. 8. Results of the simulated lifetime measurements in TRA mode of a sample with a variable number of regions of equal area each exhibiting a lifetime τ_n in between 10 and 70 µs equidistantly spaced. The case of two regions (blue) corresponds to Fig. 3. A selection of individual lifetime curves is shown in gray in steps of 10 µs for comparison.

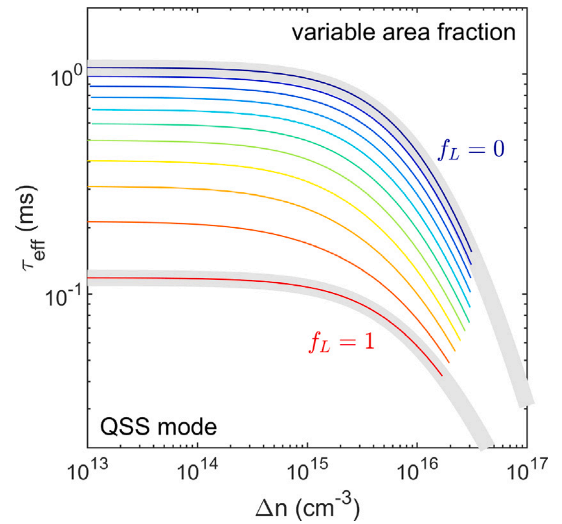

Fig. 9. Results of simulated lifetime measurements in QSS mode in the mixed region with the area fraction f_L of the low lifetime region varied from 0 (blue) to 1 (red) in steps of 0.1. The thick gray lines represent the assumed lifetimes in the regions of low ($J_{0,srf} = 100\,fA\,cm^{-2}$) and high lifetime ($J_{0,srf} = 10\,fA\,cm^{-2}$).

well above the corresponding gray line before it crosses towards the gray 30 µs line. Again, fitting such a curve with a single SRH defect is futile.

5. Inhomogeneous surface passivation

So far, lifetime differed mainly towards low injection due to differences in SRH bulk recombination. However, samples may also suffer from lateral inhomogeneous surface passivation. This issue shall now be addressed. Regions of high and low lifetime are defined by a $J_{0,srf}$ of either $10\,fA\,cm^{-2}$ or $100\,fA\,cm^{-2}$ without further bulk limitation except intrinsic recombination. The surface recombination related lifetime component (neglecting the diffusion limitation term)

$$\tau_{srf} = \frac{qwn_i^2}{2(p_0 + \Delta n)} \cdot \frac{1}{J_{0,srf}} \tag{12}$$

of a symmetrical sample of thickness w passivated by charged dielectric layers [19] features two regimes for $\Delta n \ll p_0$ (low injection) and $\Delta n \gg p_0$ (high injection). While lifetime is constant in the first, it declines with Δn^{-1} in the latter one. The common way to determine $J_{0,srf}$ is linear regression to the inverse effective lifetime (corrected for the intrinsic lifetime component τ_{int}) exploiting the $1/\tau_{srf} \propto J_{0,srf} \cdot \Delta n$ dependency as introduced by Kane and Swanson [20]. Note that the actual injection dependence of the intrinsic carrier density n_i is ignored here for reasons of simplicity, hence, the state-of-the-art $J_{0,srf}$ analysis of Kimmerle et al. [21] simplifies to the one of Kane and Swanson [20].

The simulated 'measured' effective lifetime curves for various area fractions f_L are shown in Fig. 9 for the QSS mode and in Fig. 10 for the TRA mode, respectively. Again, the lifetime curves in the individual regions are displayed as thick gray lines for comparison whereas the mixed regions are shown color-coded with area fraction f_L. In QSS mode, overall lifetime gradually changes with f_L which is a similar behavior to Fig. 12. In contrast, in TRA mode low injection lifetime converges for all f_L values to the value of the high lifetime region ($f_L = 0$) whereas τ_{eff} at higher injection $\Delta n \approx p_0$ changes gradually with f_L, implying that the lifetime curves in the mixed region do not follow the $J_{0,srf}$ behavior of Eq. (12). This can be best seen in the case of $f_L = 0.9$ (orange line) where the curve is strangely deformed around $\Delta n \sim 1 \cdot 10^{15}\,cm^{-3}$. All other lifetime curves (except f_L assuming 0 and 1) for both, the QSS and TRA mode, are deformed as well even

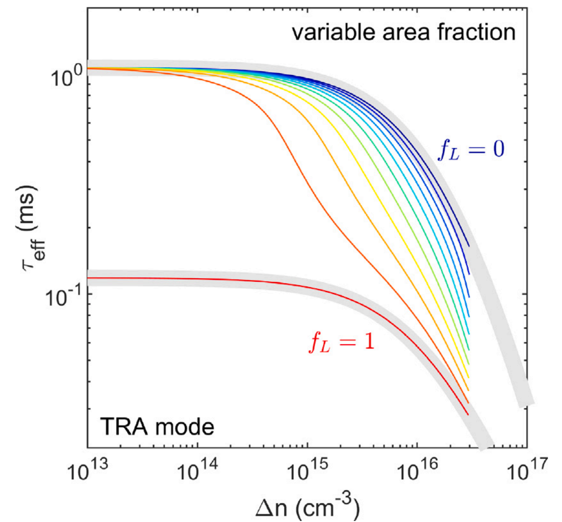

Fig. 10. Results of simulated lifetime measurements in TRA mode in the mixed region with the area fraction f_L of the high lifetime region varied from 0 (blue) to 1 (red) in steps of 0.1. The thick gray lines represent the assumed lifetimes in the regions of low ($J_{0,srf} = 100\,fA\,cm^{-2}$) and high lifetime ($J_{0,srf} = 10\,fA\,cm^{-2}$).

though it is not that obvious. This can be better seen in the plot of the inverse lifetime used for the linear regression analysis. This is exemplary depicted in Fig. 11 for the TRA mode. Due to the choice of n_i being independent of injection, the extreme cases $f_L = 0$ and $f_L = 1$ are perfectly straight lines, hence, $J_{0,srf}$ is perfectly constant with respect to injection and yields the assumed values. Or in other words, it does not matter at which injection $J_{0,srf}$ is evaluated. This holds not true for the mixed cases where the curves in Fig. 11 are somewhat bent. In principle, there is a transition in slope (and thus $J_{0,srf}$) from $10\,fA\,cm^{-2}$ (blue) to $100\,fA\,cm^{-2}$ (red). This transition occurs in case of the orange line early in the $10^{15}\,cm^{-3}$ range, but much later in the $10^{16}\,cm^{-3}$ range for the greenish/bluish curves. Hence, lateral inhomogeneity might be a reason for curve bending encountered in the $J_{0,srf}$ analysis.

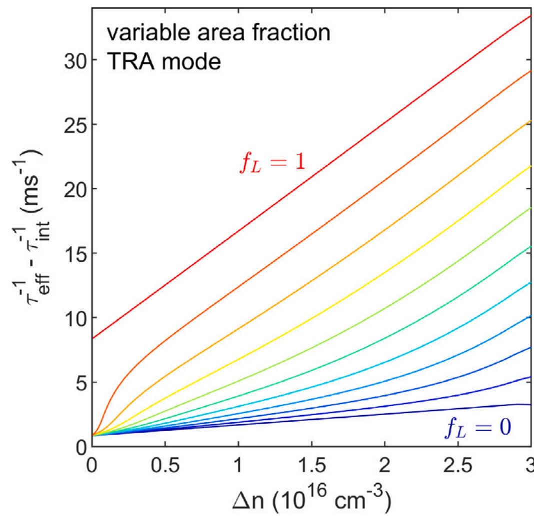

Fig. 11. Plot of the inverse effective lifetime τ_{eff} from Fig. 10 (corrected for the intrinsic lifetime component τ_{int}) used for the $J_{0,srf}$ linear regression analysis in TRA mode.

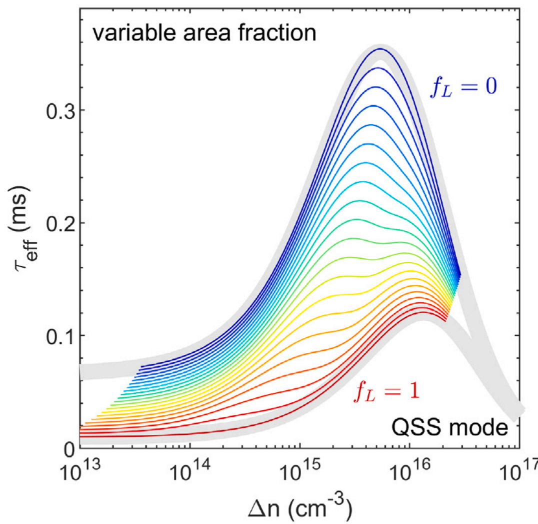

Fig. 12. Results of simulated lifetime measurements in QSS mode in the mixed region with the same parameters as in Fig. 2 except that the area fraction f_L of the low lifetime region is varied from 0 (blue) to 1 (red) in steps of 0.05. The thick gray lines represent the assumed lifetimes in the regions of low ($\tau_n = 10\,\mu s$) and high lifetime ($\tau_n = 70\,\mu s$).

6. Conclusion

Lateral inhomogeneity of the effective excess charge carrier lifetime, be it due to differences in recombination in the bulk or at the surface, may distort injection-dependent lifetime curves measured by the photoconductance decay (PCD) technique.

As demonstrated by time-dependent simulations of a sample with two regions of distinctly different lifetime and backed-up by a proof-of-principle experiment, the way these inhomogeneities impact the PCD measurement depends on the mode of operation. In particular, the presented theory describes successfully that lateral averaging occurs in the time domain, not in the injection domain, resulting in differently shaped, 'abnormal' lifetime curves in quasi steady state (QSS) or transient (TRA) mode. The generalized (GEN) mode used for lifetimes in the transition region between QSS and TRA mode exhibits features of both modes. The area fractions of high and low lifetime region are found to have an impact on the shape of the lifetime curves as well.

The transition from an abrupt lateral change in lifetime to a more gradual change results in smoother, almost non-suspicious lifetime curves that, however, do not necessarily retain the characteristics of the individual regions.

Furthermore, lateral inhomogeneities in surface passivation quality may lead to distorted lifetimes curves and might be a reason for curve bending encountered in $J_{0,srf}$ analysis.

In conclusion, the analysis of inhomogeneous samples should be treated with caution and it is certainly advisable to combine PCD lifetime measurements with imaging techniques to reliably detect issues with homogeneity and validate the correctness of PCD lifetime analysis.

CRediT authorship contribution statement

Axel Herguth: Conceptualization, Formal analysis, Investigation, Methodology, Software, Validation, Visualization, Writing – original draft. **Alexander Graf:** Conceptualization, Formal analysis, Investigation, Methodology, Software, Validation, Writing – original draft.

Declaration of competing interest

The authors declare the following financial interests/personal relationships which may be considered as potential competing interests: Axel Herguth reports financial support was provided by German Federal Ministry for Economic Affairs and Energy. If there are other authors, they declare that they have no known competing financial interests or personal relationships that could have appeared to influence the work reported in this paper.

Acknowledgments

Part of this work was funded by the German Federal Ministry for Economic Affairs and Energy (BMWE) under contract number 03EE1176C. The content is the responsibility of the authors.

Appendix. Variable area fractions

In the case of variable area fractions $f_L = (1 - f_H)$, mixed region injection in **QSS mode** (Eq. (7)) generalizes to

$$\Delta n_M(t) = (1 - f_L) \cdot \Delta n_H(t) + f_L \cdot \Delta n_L(t) \tag{13}$$

and lifetime in QSS mode (Eq. (8)) generalizes to

$$\tau_M(t) = (1 - f_L) \cdot \tau_H(t) + f_L \cdot \tau_L(t) \tag{14}$$

The resulting lifetime curves using the same parameters as in Fig. 2 but variable area fraction f_L of the low lifetime region are shown in Fig. 12. The area fraction f_L acts as a weighting factor that balances the contributions of the different regions not only to $\tau_M(t)$, but also to $\Delta n_M(t)$. This has the effect that even though the maxima of $\tau_H(t)$ and $\tau_L(t)$ do not shift in time (Fig. 2 middle), the shape of Δn_M changes. This results in an apparent shift in injection of the second maximum in Fig. 12 moving from the low 10^{14} cm^{-3} range for $f_L \sim 0.95$ to the mid 10^{15} cm^{-3} range for $f_L \sim 0.4$.

In the case of variable area fractions $f_L = (1 - f_H)$, mixed region injection in **TRA mode** (Eq. (9)) generalizes to

$$\Delta n_M(t) = (1 - f_L) \cdot \Delta n_H(t) + f_L \cdot \Delta n_L(t) \tag{15}$$

and lifetime in TRA mode (Eq. (8)) generalizes to

$$\tau_M(t) = -\frac{(1 - f_L) \cdot \Delta n_H + f_L \cdot \Delta n_L}{(1 - f_L) \cdot \frac{d\Delta n_H}{dt} + f_L \cdot \frac{d\Delta n_L}{dt}} \tag{16}$$

Note that there is in this case no common prefactor in the numerator and denominator that cancels out. The resulting lifetime curves using the same parameters as in Fig. 3 but variable area fraction f_L of the low lifetime region are shown in Fig. 13.

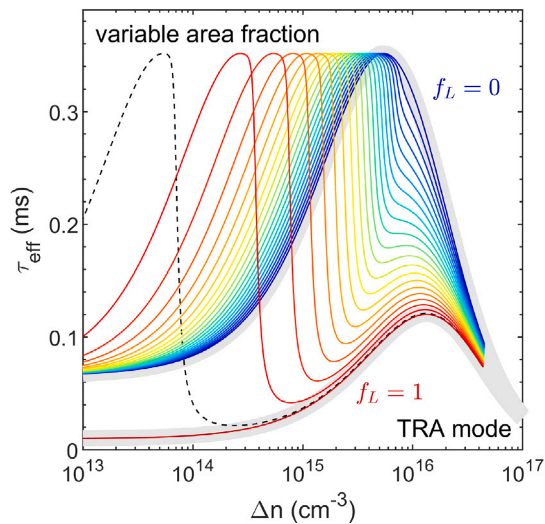

Fig. 13. Results of simulated lifetime measurements in TRA mode in the mixed region with the same parameters as in Fig. 3 except that the area fraction f_L of the low lifetime region is varied from 0 (blue) to 1 (red) in steps of 0.05. The dashed black line shows the case for $f_L = 0.99$ ($f_H = 0.01$). The thick gray lines represent the assumed lifetimes in the regions of low ($\tau_n = 10\,\mu s$) and high lifetime ($\tau_n = 70\,\mu s$).

Data availability

Data will be made available on request.

References

[1] A.B. Sproul, Dimensionless solution of the equation describing the effect of surface recombination on carrier decay in semiconductors, J. Appl. Phys. 76 (5) (1994) 2851–2854, http://dx.doi.org/10.1063/1.357521.

[2] R.A. Sinton, A. Cuevas, Contactless determination of current–voltage characteristics and minority-carrier lifetimes in semiconductors from quasi-steady-state photoconductance data, Appl. Phys. Lett. 69 (17) (1996) 2510–2512, http://dx.doi.org/10.1063/1.117723.

[3] H. Nagel, C. Berge, A.G. Aberle, Generalized analysis of quasi-steady-state and quasi-transient measurements of carrier lifetimes in semiconductors, J. Appl. Phys. 86 (11) (1999) 6218–6221, http://dx.doi.org/10.1063/1.371633.

[4] J. Giesecke, M. Schubert, B. Michl, F. Schindler, W. Warta, Minority carrier lifetime imaging of silicon wafers calibrated by quasi-steady-state photoluminescence, Sol. Energy Mater. Sol. Cells (ISSN: 0927-0248) 95 (3) (2011) 1011–1018, http://dx.doi.org/10.1016/j.solmat.2010.12.016.

[5] D. Kiliani, G. Micard, B. Steuer, B. Raabe, A. Herguth, G. Hahn, Minority charge carrier lifetime mapping of crystalline silicon wafers by time-resolved photoluminescence imaging, J. Appl. Phys. 110 (5) (2011) 054508, http://dx.doi.org/10.1063/1.3630031.

[6] L.E. Black, D.H. Macdonald, Accounting for the dependence of coil sensitivity on sample thickness and lift-off in inductively coupled photoconductance measurements, IEEE J. Photovolt. 9 (6) (2019) 1563–1574, http://dx.doi.org/10.1109/jphotov.2019.2942484.

[7] N.E. Grant, F.E. Rougieux, D. Macdonald, J. Bullock, Y. Wan, Grown-in defects limiting the bulk lifetime of p-type float-zone silicon wafers, J. Appl. Phys. 117 (5) (2015) http://dx.doi.org/10.1063/1.4907804.

[8] D. Bredemeier, D. Walter, S. Herlufsen, J. Schmidt, Understanding the light-induced lifetime degradation and regeneration in multicrystalline silicon, Energy Procedia 92 (2016) 773–778, http://dx.doi.org/10.1016/j.egypro.2016.07.060.

[9] A.E. Morishige, M.A. Jensen, D.B. Needleman, K. Nakayashiki, J. Hofstetter, T.-T.A. Li, T. Buonassisi, Lifetime spectroscopy investigation of light-induced degradation in p-type multicrystalline silicon PERC, IEEE J. Photovolt. 6 (6) (2016) 1466–1472, http://dx.doi.org/10.1109/jphotov.2016.2606699.

[10] K. Nakayashiki, J. Hofstetter, A.E. Morishige, T.-T.A. Li, D.B. Needleman, M.A. Jensen, T. Buonassisi, Engineering solutions and root-cause analysis for light-induced degradation in p-type multicrystalline silicon PERC modules, IEEE J. Photovolt. 6 (4) (2016) 860–868, http://dx.doi.org/10.1109/jphotov.2016.2556981.

[11] T. Niewelt, F. Schindler, W. Kwapil, R. Eberle, J. Schön, M.C. Schubert, Understanding the light-induced degradation at elevated temperatures: Similarities between multicrystalline and floatzone p-type silicon, Prog. Photovolt., Res. Appl. 26 (8) (2017) 533–542, http://dx.doi.org/10.1002/pip.2954.

[12] T. Niewelt, M. Selinger, N.E. Grant, W. Kwapil, J.D. Murphy, M.C. Schubert, Light-induced activation and deactivation of bulk defects in boron-doped float-zone silicon, J. Appl. Phys. 121 (18) (2017) http://dx.doi.org/10.1063/1.4983024.

[13] D. Sperber, A. Graf, D. Skorka, A. Herguth, G. Hahn, Degradation of surface passivation on crystalline silicon and its impact on light-induced degradation experiments, IEEE J. Photovolt. 7 (6) (2017) 1627–1634, http://dx.doi.org/10.1109/jphotov.2017.2755072.

[14] T. Niewelt, B. Steinhauser, A. Richter, B. Veith-Wolf, A. Fell, B. Hammann, N. Grant, L. Black, J. Tan, A. Youssef, J. Murphy, J. Schmidt, M. Schubert, S. Glunz, Reassessment of the intrinsic bulk recombination in crystalline silicon, Sol. Energy Mater. Sol. Cells 235 (2022) 111467, http://dx.doi.org/10.1016/j.solmat.2021.111467.

[15] D. Macdonald, A. Cuevas, Trapping of minority carriers in multicrystalline silicon, Appl. Phys. Lett. (ISSN: 1077-3118) 74 (12) (1999) 1710–1712, http://dx.doi.org/10.1063/1.123663.

[16] T. Niewelt, J. Schon, W. Warta, S.W. Glunz, M.C. Schubert, Degradation of crystalline silicon due to boron-oxygen defects, IEEE J. Photovolt. 7 (1) (2017) 383–398, http://dx.doi.org/10.1109/jphotov.2016.2614119.

[17] A. Herguth, B. Hallam, A generalized model for boron-oxygen related light-induced degradation in crystalline silicon, in: AIP Conference Proceedings, vol. 1999, AIP Publishing, 2018, 130006, http://dx.doi.org/10.1063/1.5049325.

[18] J. Schmidt, D. Bredemeier, D.C. Walter, On the defect physics behind light and elevated temperature-induced degradation (LeTID) of multicrystalline silicon solar cells, IEEE J. Photovolt. 9 (6) (2019) 1497–1503, http://dx.doi.org/10.1109/jphotov.2019.2937223.

[19] K.R. McIntosh, L.E. Black, On effective surface recombination parameters, J. Appl. Phys. 116 (1) (2014) 014503, http://dx.doi.org/10.1063/1.4886595.

[20] D. Kane, R. Swanson, Measurement of the emitter saturation current by a contactless photoconductivity decay method, in: Proceedings of 1985 IEEE Photovoltaic Specialists Conference, 1985, pp. 578–583.

[21] A. Kimmerle, J. Greulich, A. Wolf, Carrier-diffusion corrected J0-analysis of charge carrier lifetime measurements for increased consistency, Sol. Energy Mater. Sol. Cells 142 (2015) 116–122, http://dx.doi.org/10.1016/j.solmat.2015.06.043.